In-situ QXAS study of sulfidation/oxidative regeneration reactions of zinc molybdate ZnMoO 4 and ZnO-MoO 3 materials

Vincent Girard, David Chiche, Arnaud Baudot, Delphine Bazer-Bachi, Laurent Lemaître, Virginie Moizan-Baslé, Amélie Rochet, Valérie Briois, Christophe Geantet

In-situ QXAS study of sulfidation/oxidative regeneration reactions of zinc molybdate $ZnMoO_4$ and ZnO-MoO_3 materials

*Vincent Girard,[1, 3] David Chiche,[1] Arnaud Baudot,[1] Delphine Bazer-Bachi,[1] Laurent Lemaitre,[1] Virginie Moizan-Baslé,[1] Amélie Rochet,[2] Valérie Briois,[2] Christophe Geantet[3]**

[1]IFP Energies nouvelles, Rond-point de l'échangeur de Solaize, BP3, 69360 Solaize, France

[2]Synchrotron SOLEIL, L'Orme des Merisiers, BP 48, Saint Aubin, 91192 Gif sur Yvette, France

[3]Université de Lyon, Institut de Recherches sur la Catalyse et l'Environnement de Lyon (IRCELYON), UMR5256 CNRS – UCB de Lyon I, 2 avenue Albert Einstein, 69626 Villeurbanne cedex, France

* To whom correspondence should be addressed. E-mail: christophe.geantet@ircelyon.univ-lyon1.fr

Abstract

Recent technologies such as those using coal, natural gas or biomass as a fuel are often facing the challenge of removing H_2S impurities. Among the various existing routes for performing sulfur removal, the conversion of transition metal oxides into sulfides is often considered for deep gas purification. The ideal regenerative system, preventing wastes, should combine a high affinity material towards H_2S and an easy way to be regenerated into its initial oxide form. The present paper describes the reactivity of $ZnMoO_4$ mixed oxide material and of a ZnO-MoO_3 oxides mixture, as potential candidates for regenerative H_2S sorption process. The use of QXAS technique allowed for getting time resolved information on both sulfidation and oxidative regeneration processes at Mo and Zn K-edges. Facing the complexity of gas-solid reactions involving several phases, QXAS combined to multivariate data analysis enabled to follow sulfidation and oxidative regeneration kinetics of both materials, with a description of the evolution of the several intermediate phases. Both Mo and Zn K-edges spectroscopic data were analyzed and comparison of the evolution of ternary oxides containing the two elements is a strong argument for validating the results.

1. Introduction

Integrated Gasification Combined Cycles (IGCC) power generation processes and Fischer-Tropsch based XTL processes (XTL for X=Biomass, Coal, or Gas To Liquids) constitute efficient and cleaner alternative technologies for future energy production [1–3]. Both technologies are based on a first step of feed gasification into a synthesis gas or syngas, composed mainly of a mixture of CO and H_2 [4]. In IGCC processes, the syngas is burnt into a gas turbine to produce power. In the XTL processes, the syngas is converted into hydrocarbon fuel through the Fischer-Tropsch reaction [5–7]. Hydrogen sulfide constitutes one of the main impurities of synthesis gases [8]. On one hand, this compound mixed to H_2, is responsible for the corrosion of the industrial units [9], especially the combustion turbine blades used in the IGCC power plants. On another hand, it is also a poison of Fischer-Tropsch catalysts (cobalt-, iron-, and ruthenium-based) because of its irreversible chemisorption on their active sites [10–12]. Therefore, the sulfur content specifications in syngas are very drastic for such industrial units, below 10 ppmv for IGCC processes [13,14], and 0.05 ppmv for XTL processes [15,16]. Syngas bulk desulfurization is commonly conducted by chemical or physical solvents [8,17,18], though these technologies do not allow to achieve complete

H_2S removal. Indeed, expected H_2S syngas content at solvent-based acid gas removal systems outlet (in the range 0.1 – 1 mol. ppm) remains higher than sulfur syngas content tolerated at Fischer-Tropsch process inlet [8,11]. Therefore deep desulfurization of syngas is generally achieved with solid sorbents based on metal oxides which can irreversibly react with H_2S to form corresponding sulfide phases according to the following generic reaction:

$$M_xO_y(s) + y\ H_2S(g) \rightarrow M_xS_y(s) + y\ H_2O(g)$$

Because of the important and various initial amounts of H_2S (1 to 10000 ppm) [19], the drastic sulfur specifications required, and the large syngas flow rates to be treated (around 100 $kg.s^{-1}$ for an IGCC power plant) [20], the use of metal oxides based sorbents imposes either huge amounts of solids with large reactor or the use of small reactors and frequent changes of solid sorbent. In both cases, the large amount of solid waste produced is the major drawback of the sorbent-based syngas desulfurization, and may also alter process operation, efficiency, and economics. The *in-situ* regeneration of the sulfided sorbent, back to the oxide phase, is an identified solution to improve desulfurization processes [21–24]. SO_2 released during the regeneration step is also a harmful gas which requires to be removed. SO_2 containing gas can be handled using many different processes, such as the use of natural low-cost scavenger (*e.g.* limestone), or can be concentrated using regenerable process such as some specific solvent based acid gas removal processes (*e.g.* Cansolv process), and eventually converted in sulfur through Claus catalytic process [17].

In previous studies [25,26], zinc molybdate phase ($ZnMoO_4$) was found to exhibit high sulfur uptake capacity and to be regenerable during thermogravimetric experiments at a relatively low temperature (500°C) as compared to other metal oxide based sorbents reported in the literature [27–29]. Reactions involved during the sulfidation and oxidative regeneration of $ZnMoO_4$ materials were studied by *in-situ* X-Ray Diffraction (XRD) [26]. However, the reaction kinetics are too fast for the time resolution of laboratory XRD diffractometer; consequently the reactions dynamic cannot be precisely studied. Introduced in the late 1980's, time resolved synchrotron methods such as QXAS (Quick-scanning X-ray Absorption Spectroscopy) [30,31] are now well established techniques providing structural information with time resolutions in the range of milliseconds or seconds. Therefore, the aim of the present work is two-fold: to study the dynamic of the $ZnMoO_4$ structural evolution during sulfidation and oxidative regeneration by time resolved QXAS, and to determine the reaction mechanisms that are involved in the complete regeneration of the sulfided $ZnMoO_4$. These results will be compared to the ones obtained with the ZnO-MoO_3 physical mixture demonstrating the benefit of using the ternary oxide phase. Moreover, the performance of

QXAS beamline and the accumulation of data require new data treatment approaches such as Multivariate Curve Resolution methodology.

2. Materials and Methods

2.1 Composite oxides syntheses

The single oxides mixture ZnO-MoO_3 (atomic ratio Zn/Mo=1) was obtained by physical milling of MoO_3 and ZnO materials. ZnO material was synthesized from thermal decomposition of precursor at 500°C for 2 hours. The precursor was $(ZnCO_3)_2 \cdot (Zn(OH)_2)_3$ (Aldrich, purity > 58% Zn). MoO_3 precursor was obtained from a chemical supplier (Aldrich, purity > 99.5%), and was used as received after material characterizations. $ZnMoO_4$ mixed oxide phase was synthesized by successive calcination steps under air atmosphere at 400°C for 48h and 500°C for 12h and physical milling of the previous ZnO-MoO_3 single oxides mixture. $ZnMoO_3$ reference was obtained from reduction of $ZnMoO_4$ at 400°C, for 6 hours under pure hydrogen flow.

2.2 *In-situ* X-ray Absorption Spectroscopy experiments

QXAS measurements were carried out on the SAMBA beamline at SOLEIL synchrotron [32]. Si(111) and Si(311) channel-cut crystals were used as monochromator for the Zn and Mo K-edges, respectively. The Si(111) and Si(311) channel-cut crystals were tuned to a Bragg angle of 12.1° (with a crystal oscillation amplitude of 1.4°) and 10.8° (with a crystal oscillation amplitude of 0.7°), respectively. The monochromators were calibrated by setting the first inflection point of the K-edge spectrum of two standard Mo and Zn metal foils at, respectively, 20000 eV and 9659 eV. For both edges, a frequency of 1 Hz was used for the crystal oscillation to obtain each second two spectra (one for increasing, the other for decreasing Bragg angles). This oscillation frequency was sufficient to get an adequate time resolution for the studied reactions. The energy resolution is related to the Renishaw encoders resolution modulated by the rise time of electronics used for signal detection. At the sampling rate of 1 Hz used herein, no limitation is associated to the electronics and an oversampling of angle values is obtained. Consequently the raw energy grid of the recorded data is further interpolated with energy step at the Zn K-edge of 2 eV from 9400 to 9620 eV, 0.3 eV from 9620 to 9800 and 2 eV above 9800 eV, and, at the Mo K-edge of 0.8 eV from 19810 to 20200 eV and 2 eV above 20200 eV.

Harmonic rejection was achieved by using the two Pd coated mirrors available on the SAMBA beamline. XAS spectra were measured in transmission mode with three OKEN ionization chambers (IC) filled with N_2 for the Zn K-edge measurements and with Ar at the Mo K-edge. The sulfidation and oxidative regeneration reactions were followed by QXAS by using a dedicated cell connected to the gas feeding system installed on the SAMBA beamline [33]. The exhaust gases were collected into the dangerous gases network of the beamlines. The gas cylinders were stored into a ventilated cabinet located inside the experimental hutch close to the reactor for limiting the length of tubing containing gases. Before introducing H_2S a leak test was carried out under helium using a portable He leak detector. The beamline was equipped of permanent leak detectors for H_2S to quickly react to any leak of H_2S which could result from break of one of the X-rays window used in the reactor. To achieve the desired sample absorption, the cavity of the sample holder was filled with two different material amounts: 20 and 10 mg of solids were respectively used for the experiments at the molybdenum and zinc K-edges.

After heating to 350°C under a He flow, the sulfidation of the oxide materials was performed at 350°C with a 0.9% H_2S in H_2 gas mixture under a constant flow rate (1 $NmL.min^{-1}.mg^{-1}$ of solid material, equivalent to 0.1 mol of $H_2S.min^{-1}.mol^{-1}$ of $ZnMoO_4$ or $ZnO\text{-}MoO_3$). This step lasted 3 hours for the $ZnO\text{-}MoO_3$ physical mixture and 2 hours for the $ZnMoO_4$ material.

At the end of this step, the gas mixture was switched to a N_2 flow (20 $NmL.min^{-1}$), and the reactor was heated up to 500°C, the regeneration temperature. After temperature stabilization, the gas was switched to the oxidative gas mixture (5% O_2 in N_2) during 2 hours at a constant flow rate (1 $NmL.min^{-1}.mg^{-1}$ of solid material, equivalent to 0.5 mol of $O_2.min^{-1}.mol^{-1}$ of $ZnMoO_4$ or $ZnO\text{-}MoO_3$). For dynamic studies, twenty spectra with upwards Bragg angles were merged to improve the signal-to-noise ratio.

Energy calibration and normalization of the QXAS raw data have been carried out using the normal_gui Python interface developed at SOLEIL [34]. Then the normalized μ(E) QXAS spectra recorded during the sulfidation/regeneration procedure were investigated by multivariate data analysis enabling to handle the huge amount of data [35]. More details regarding the Multivariate Curve Resolution with Alternating Least Squares (MCR-ALS) fitting methodology applied to XAS spectra can be found in [36–39]. MCR-ALS minimization was performed on MATLAB© using the graphical user interface MCR-ALS GUI 2.0 developed by *Jaumot et al* [40,41]. MCR-ALS pure spectra species can be compared to different references of freshly prepared $ZnMoO_4$, $ZnMoO_3$ and ZnO, ZnS (obtained from

sulfided ZnO), commercial MoO_3 and MoO_2 materials, MoS_2 previously recorded [42]. Molybdenum and zinc metal foils were used for energy calibration. Concentration profiles extracted from MCR-ALS contain hundreds of data points and for simplification are represented by a moving average trend line.

3. Results and Discussion

The XANES spectra at Mo K-edge and Zn K-edge of the reference materials presented in Fig. 1 illustrates the sensitivity of XANES spectroscopy which can clearly discriminate the solid phases involved during the sulfidation and regeneration steps.

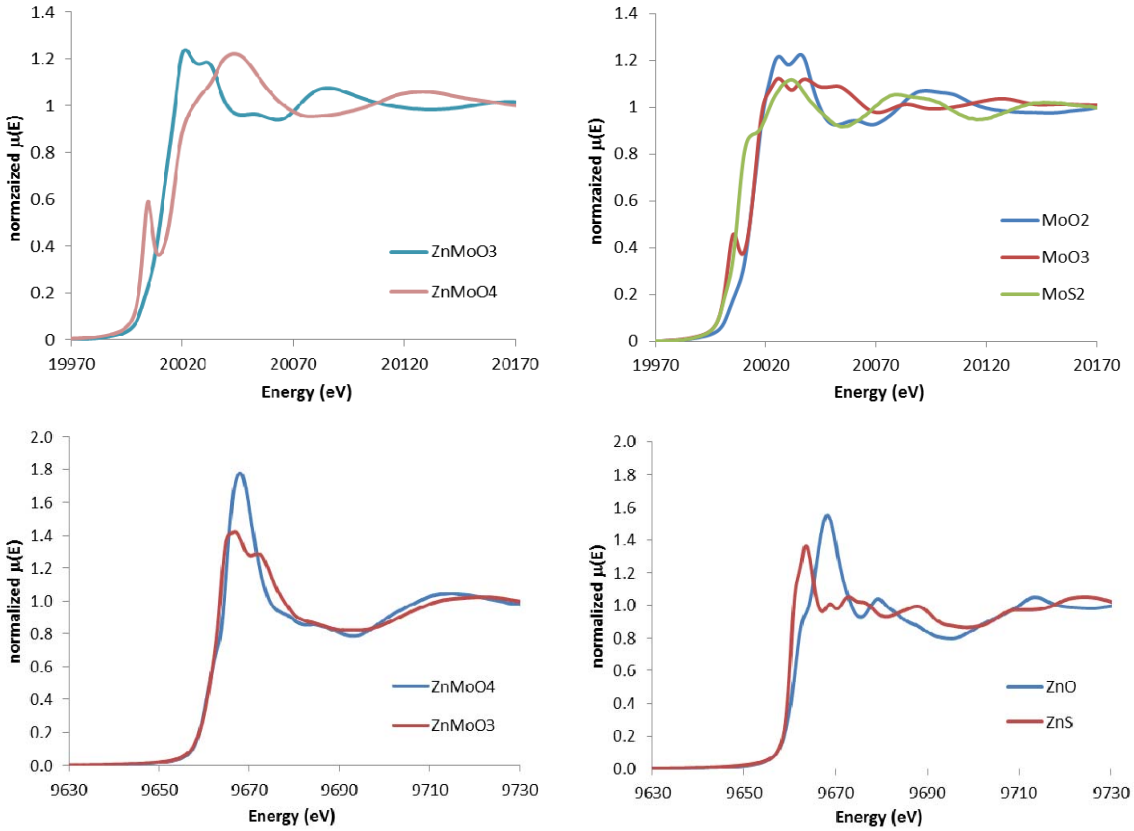

Fig. 1. Reference compounds XANES spectra at Mo K-edge (up) and Zn K-edge (down).

The different features of the molybdenum atoms in various oxidation states exhibit characteristic line shapes at the edge as well as energy shifts as reported in literature [43–47]. Thus, at Mo K-edge, pre-edge features due to the forbidden transition from *s* to *d* levels, observable because of a mixing of *d* and *p* orbitals of Mo^{VI} in tetrahedral or highly distorted octahedral environment, are well identified on α-$ZnMoO_4$ [48] and MoO_3 spectra [43,44].

XANES spectrum of $ZnMoO_4$ has been only reported for Mo L_{III}-edge [49]. At Zn K-edge, whatever the type of compound, no pre-edge features are observed due to the full occupancy of Zn *d* orbitals. The XANES spectra observed in ZnO and both wurtzite and sphalerite ZnS structures have been already studied and modeled [50,51]. ZnS reference material was obtained from complete sulfidation under H_2S of the ZnO reference material. As reported previously for ZnS [52], three characteristic peaks are observed up to 50 eV above the Zn K-edge. The Zn K edge XANES spectra of $ZnMoO_4$ and $ZnMoO_3$ are reported for the first time herein. Note that this latter oxide does not belong to ilmenite family ($FeTiO_3$) but to a defective spinel class. According to the cation distribution classification proposed by *Manthiram et al* [53] from the XRD intensity ratio of (400) and (200) peaks, the cation distribution of our reference compounds is $Zn_t[Zn_{1/3}Mo_{4/3}\square_{1/3}]_oO_4$ (in which □ denotes cation vacancy and t and o tetrahedral and octahedral sites of the spinel structure). Considering the strong versatility of this metastable phase, one can expect some discrepancies in the XANES spectra of the reference material and the one extracted from MCR-ALS since operating conditions for sulfidation/regeneration reactions studied and reference material synthesis conditions might differ.

All the reference compounds exhibit well defined resolved XANES features and allowing us to discriminate the evolution of reactants during sulfidation and regeneration through MCR-ALS analysis. These reference compounds have been compared to the mathematical solutions proposed by MCR-ALS analysis, as presented in Supporting Information. The comparison of the spectra of species extracted by MCR-ALS and references is good for most of the species involved in the process (ZnO, ZnS, $ZnMoO_4$ at both edges, MoO_2, MoO_3). We had to use spectra of references into the MCR-ALS minimization only for $ZnMoO_3$ and MoS_2 phases, as discussed in Supporting Information.

In-situ **sulfidation experiments**

The XANES spectra evolutions at both Mo and Zn K-edges observed during the sulfidation of ZnO-MoO_3 physical mixture and $ZnMoO_4$ material are presented in Fig. 2 and Fig. 3, respectively. Irrespective the materials, a fade-out of the pre-edge intensity at the Mo K-edge can be observed. Moreover, the energy downshift of the Mo K-edge is characteristic of the reduction of the oxidation state of molybdenum [43–45,47]. In agreement with previously reported *in-situ* XRD characterizations [26], this trend also indicates the formation of reduced Mo species such as MoS_2 and MoO_2 and $ZnMoO_3$ from $ZnMoO_4$ starting material, and MoO_2 and MoS_2 from the ZnO-MoO_3 mixture. The MCR-ALS determination of the spectra of pure

species, over the full collected energy range, of the experiment during the sulfidation of both Zn-based materials can be compared to the reference compounds (see Supporting Information). The chemometric method can clearly discriminate ZnO, ZnS, $ZnMoO_4$ and $ZnMoO_3$ contributions at Zn K-edge, and MoO_3, MoO_2, MoS_2, $ZnMoO_4$ and $ZnMoO_3$ at Mo K-edge. Details about the MCR-ALS resolution of sulfidation treatments at both edges of ZnO:MoO_3 50:50 mixture and $ZnMoO_4$ materials can be found in Supplementary Information. It can be noted that upon heating treatment to the temperature (350°C) at which sulfidation is carried out, a faint transformation of ZnO:MoO_3 into $ZnMoO_4$ (≈ 10% at the Mo K edge or less at the Zn K edge) occurs before introducing H_2S, resulting probably from air captured in the bypass valve when it was used for isolating the reactor for filling the gas lines.

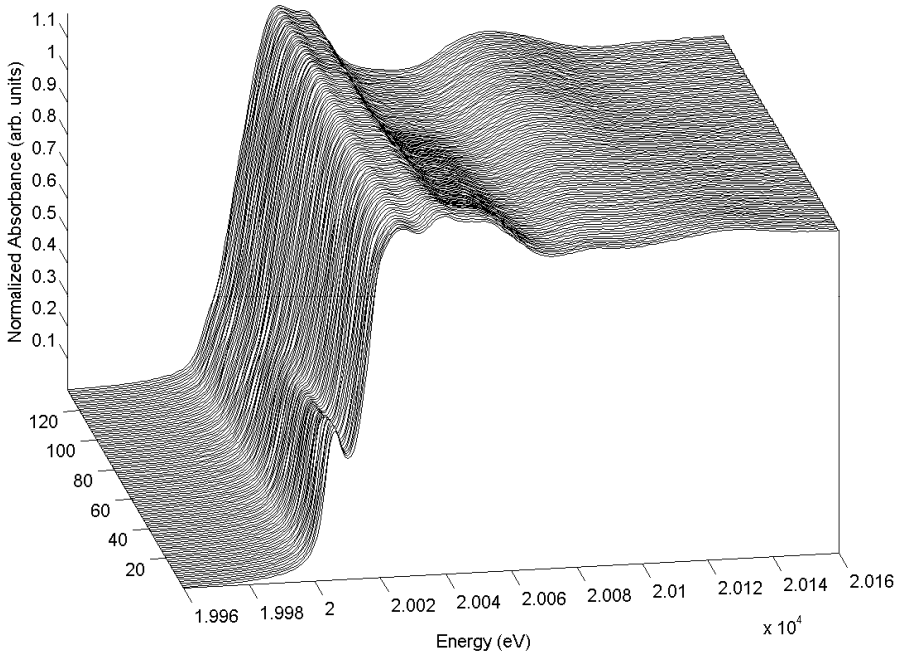

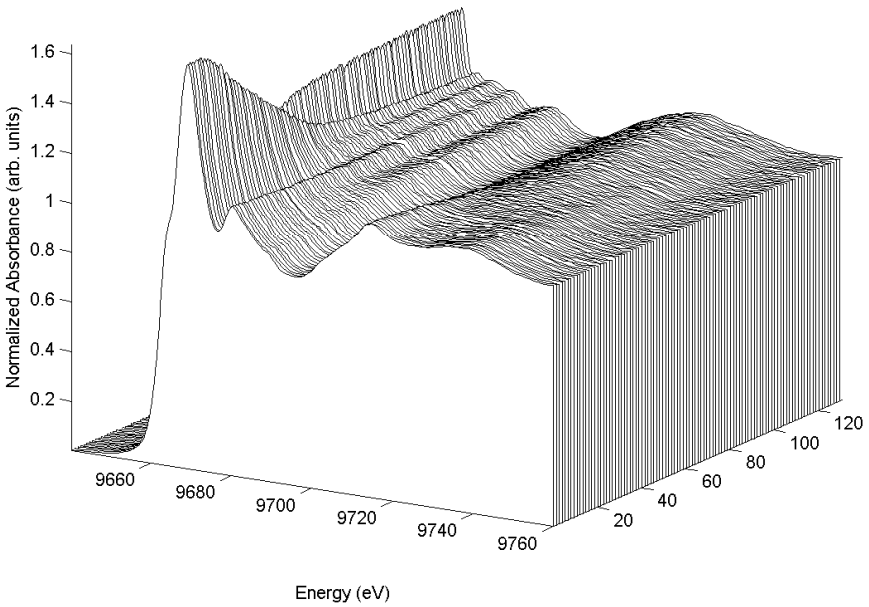

Fig. 2. Evolutions of time-resolved XANES spectra at Mo K-edge (up) and Zn K-edge (down) during the *in-situ* sulfidation of the ZnO-MoO_3 material physical mixture, under 0.9% H_2S in H_2 at 350°C.

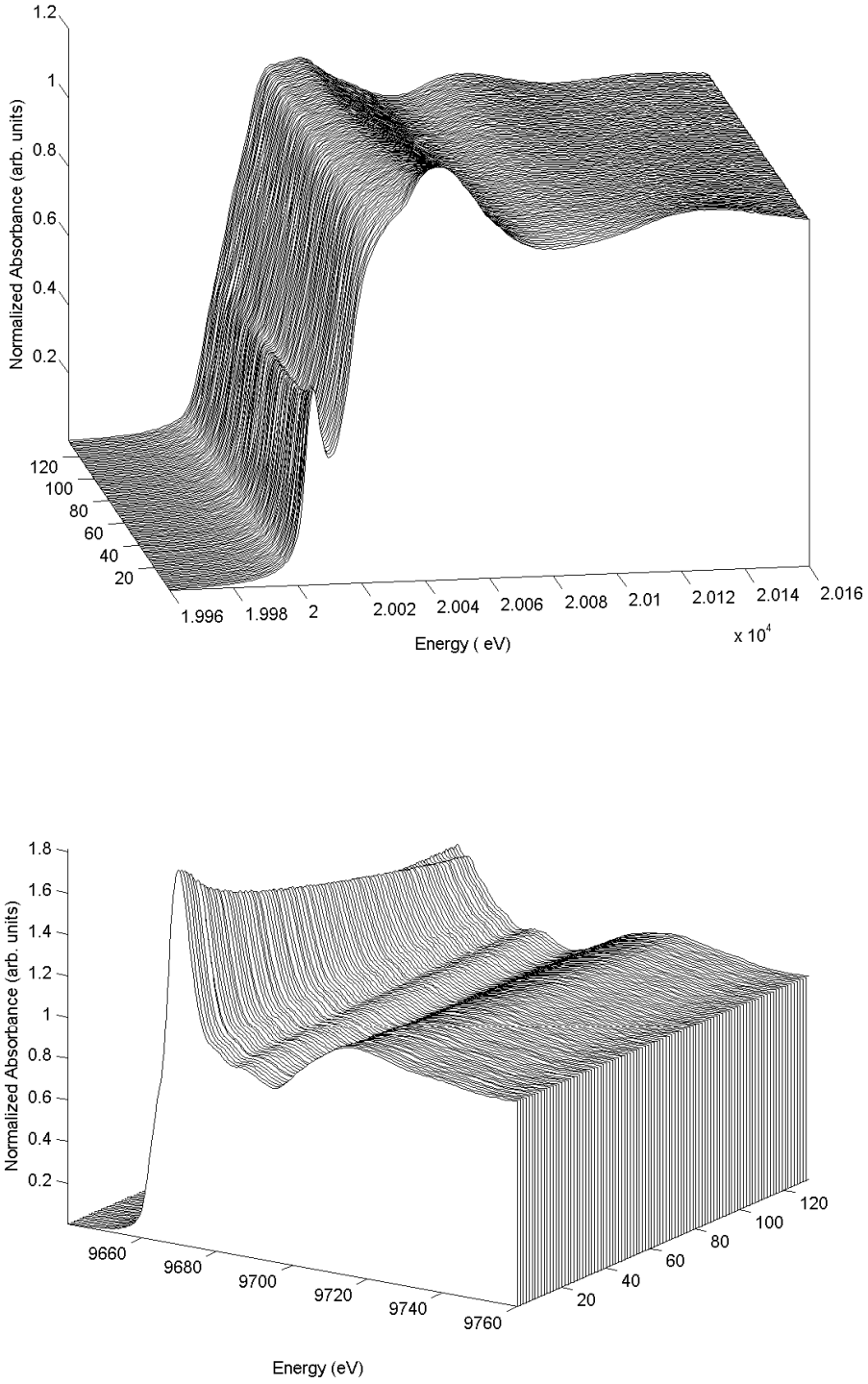

Fig. 3. Evolutions of time-resolved XANES spectra at Mo K-edge (up) and Zn K-edge (down) during the *in-situ* sulfidation of $ZnMoO_4$ material, under 0.9% H_2S in H_2 at 350°C.

The concentration profiles obtained from MCR-ALS methodology applied to the XAS spectra recorded at both Mo and Zn K-edges during the sulfidation procedure of the ZnO-MoO_3 physical mixture are reported on Fig. 4 and Fig. 5, respectively.

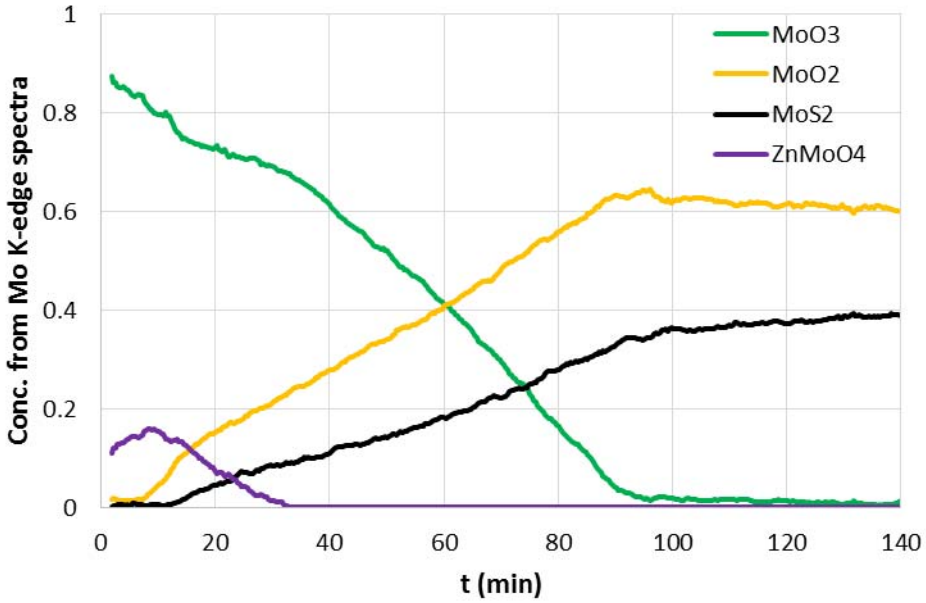

Fig. 4. MCR-ALS determination of concentration profiles as a function of time of Mo containing compounds (QXAS at Mo K-edge, 539 spectra) during the sulfidation of MoO_3-ZnO mixture.

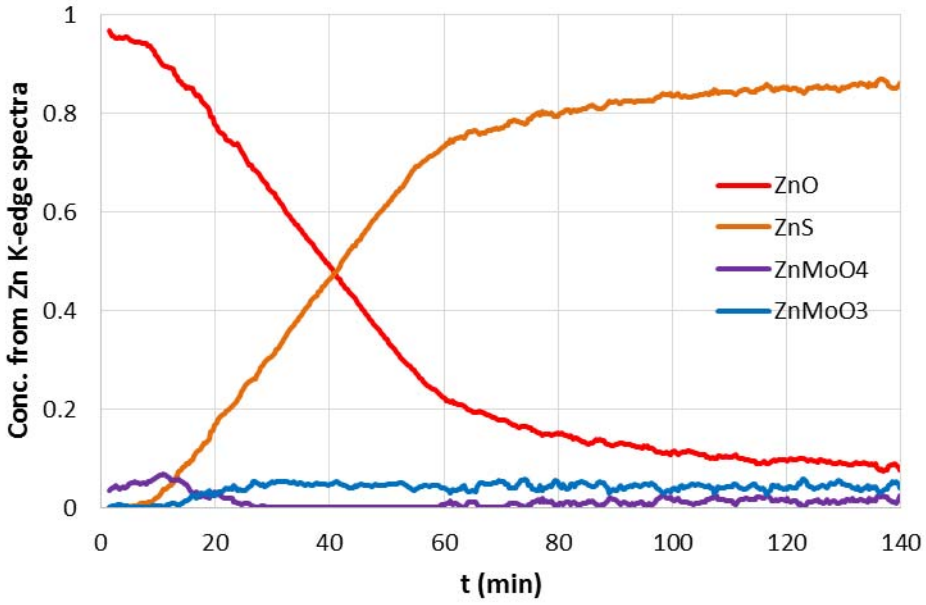

Fig. 5. MCR-ALS determination of concentration profiles as a function of time of Zn containing compounds (QXAS at Zn-K-edge, 539 spectra) during the sulfidation of MoO_3-ZnO mixture.

The sulfidation of the MoO_3 particles in the ZnO-MoO_3 mixture results in the formation of MoS_2 and MoO_2 phases (see Fig. 4). Previous studies demonstrated that MoO_3 sulfidation occurs at the particle surface, whereas particle core is reduced into MoO_2 [54,55].

Independently, ZnS phase is formed during the sulfidation step from ZnO particles present in the ZnO-MoO_3 mixture (see Fig. 5). MCR-ALS also identifies the appearance of ~5% $ZnMoO_3$ during the sulfidation process of ZnO-MoO_3 mixture from Zn K-edge spectra (Fig. 5), but not from Mo K-edge spectra (Fig. 4). However, this signal cannot be considered as significant for such low amounts detected, and therefore the presence of $ZnMoO_3$ is not attested. This phase composition evolution during the sulfidation process is in agreement with previously reported *in-situ* XRD experiments carried out the same materials [26]. ZnO particle sulfidation mechanism and kinetics are also well known. It occurs through an outward growth development of the ZnS phase over ZnO particles, due to zinc and oxygen atoms diffusion through the outer layer [56,57]. This reaction also shows important kinetic limitations, leading to a incomplete conversion of ZnO phase. The sulfidation reactions involved with the ZnO-MoO_3 mixture are the following:

$$ZnO(s) + H_2S(g) \rightarrow ZnS(s) + H_2O\ (g) \quad (5)$$

$$2\ MoO_3(s) + 2\ H_2S(g) + 2\ H_2(g) \rightarrow MoO_2(s) + MoS_2(s) + 4\ H_2O\ (g) \quad (6)$$

Reaction 6 is completed after 100 min, with 60% of MoO_2 and 40% of MoS_2 as reaction products. This ratio depends on the size of starting MoO_3 platelets.

Consequently, the reactivity of the ZnO-MoO_3 single oxides mixture is similar to the reactivity of the separated single oxides without formation of any mixed phase.

The concentration profiles evolution during the $ZnMoO_4$ material sulfidation stage are reported on Fig. 6 and Fig. 7 for Mo K-edge and Zn K-edge measurements respectively.

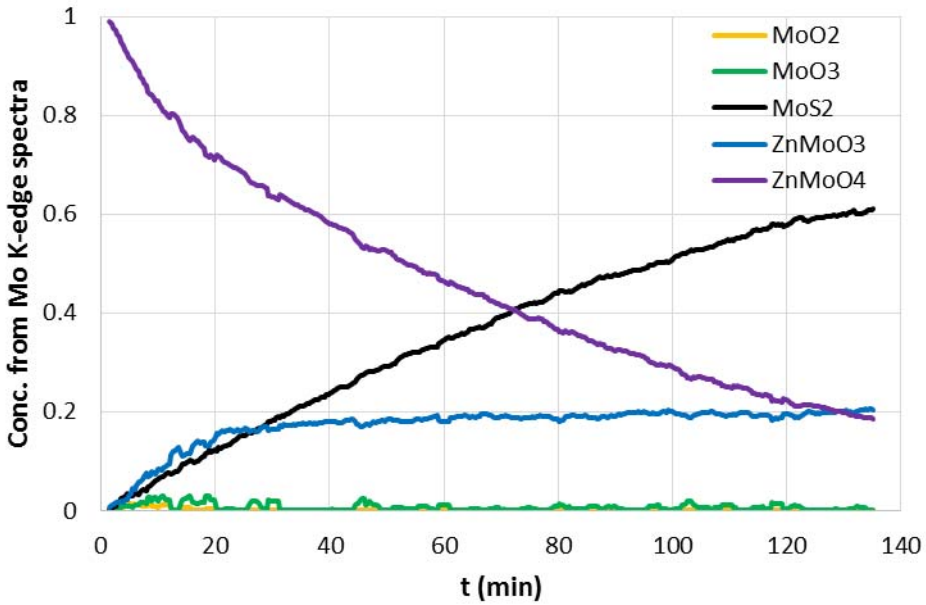

Fig. 6. MCR-ALS determination of concentration profiles as a function of time for Mo compounds (QXAS at Mo K-edge, 406 spectra) during the sulfidation of $ZnMoO_4$ starting material.

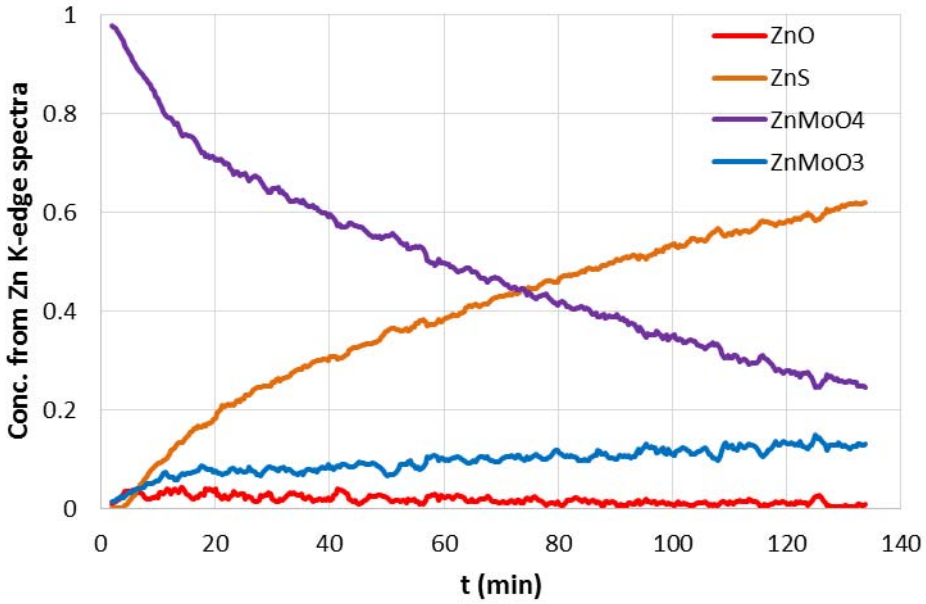

Fig. 7. MCR-ALS determination of concentration profiles as a function of time for Zn compounds (QXAS at Zn K-edge, 401 spectra) during the sulfidation of $ZnMoO_4$ starting material.

Through the comparison of data reported on Fig. 6 and Fig. 7, one can notice the good agreement of the two edges analysis with respect to $ZnMoO_4$ consumption as well as concomitant increase of MoS_2 and ZnS content, thus validating the multivariate analysis method. A small discrepancy in the total amount of the side reaction producing $ZnMoO_3$ (related to $ZnMoO_4$) at the two different edges is observed. This may originate from the discrimination of the two spectra during multivariate analysis. At Mo K-edge more differences are observed suggesting a more reliable result than at Zn K-edge (Fig. 1).

Previously, based on XRD and TEM qualitative analysis, we proposed the following global reaction for the sulfidation of $ZnMoO_4$ phase:

$$2\ ZnMoO_4(s) + 3\ H_2S(g) + 2\ H_2(g) \rightarrow ZnS(s) + MoS_2(s) + ZnMoO_3(s) + 5\ H_2O(g) \qquad (1)$$

The sulfidation of the mixed oxide $ZnMoO_4$ phase led to a phase demixing, into a ZnS shell and a MoS_2 and $ZnMoO_3$ core as shown from TEM observations reported in a previous work [26]. This phase demixing involves solid-state diffusion phenomena to proceed, and, as in the case of ZnO sulfidation (in ZnO-MoO_3 mixture), this leads to strong kinetic limitations

responsible for an incomplete conversion of the initial oxide phase. This QXAS study gives a better insight of this process and allows us to propose competitive mechanisms, showing $ZnMoO_4$ consumption resulting from parallel sulfidation and reduction reactions. The following sulfidation reaction is shown to occur:

$$ZnMoO_4(s) + 3\ H_2S(g) + H_2(g) \rightarrow ZnS(s) + MoS_2(s) + 4\ H_2O(g) \quad (2)$$

$ZnMoO_4$ reduction proceeds according to the following reaction:

$$ZnMoO_4(s) + H_2(g) \rightarrow ZnMoO_3(s) + H_2O(g) \quad (3)$$

Indeed, according to Mo K-edge analysis, $ZnMoO_3$ is mainly formed at the early stage of the reaction (t = 0 to 20 min), and its formation is then considerably slowed. Similar trend is observed from Zn K-edge analysis, and $ZnMoO_3$ seems to be formed from a parallel route as sulfide species are produced. These observations are similar to previous mechanisms proposed for MoO_3 sulfidation under a H_2S/H_2 atmosphere, leading to MoS_2 slabs formation over the surface of reduced MoO_2 particle [58].

In-situ regeneration experiments

The XANES spectra evolutions at both Mo and Zn K-edges observed during the regeneration stage of sulfided ZnO-MoO_3 mixture and $ZnMoO_4$ materials are presented in Fig. 8 and Fig. 9, respectively. During the regeneration at Mo K-edge, an edge shift to higher values as well as the rapid occurrence of a pre-edge characteristic of molybdenum atoms Mo^{VI} in a tetrahedral or distorted octahedral environment [43–45] are observed for both materials, consistent with the formation of $ZnMoO_4$ and/or MoO_3 phases. Chemometric analysis allows us to discriminate the compounds distribution and distinguish $ZnMoO_4$ and MoO_3 contributions.

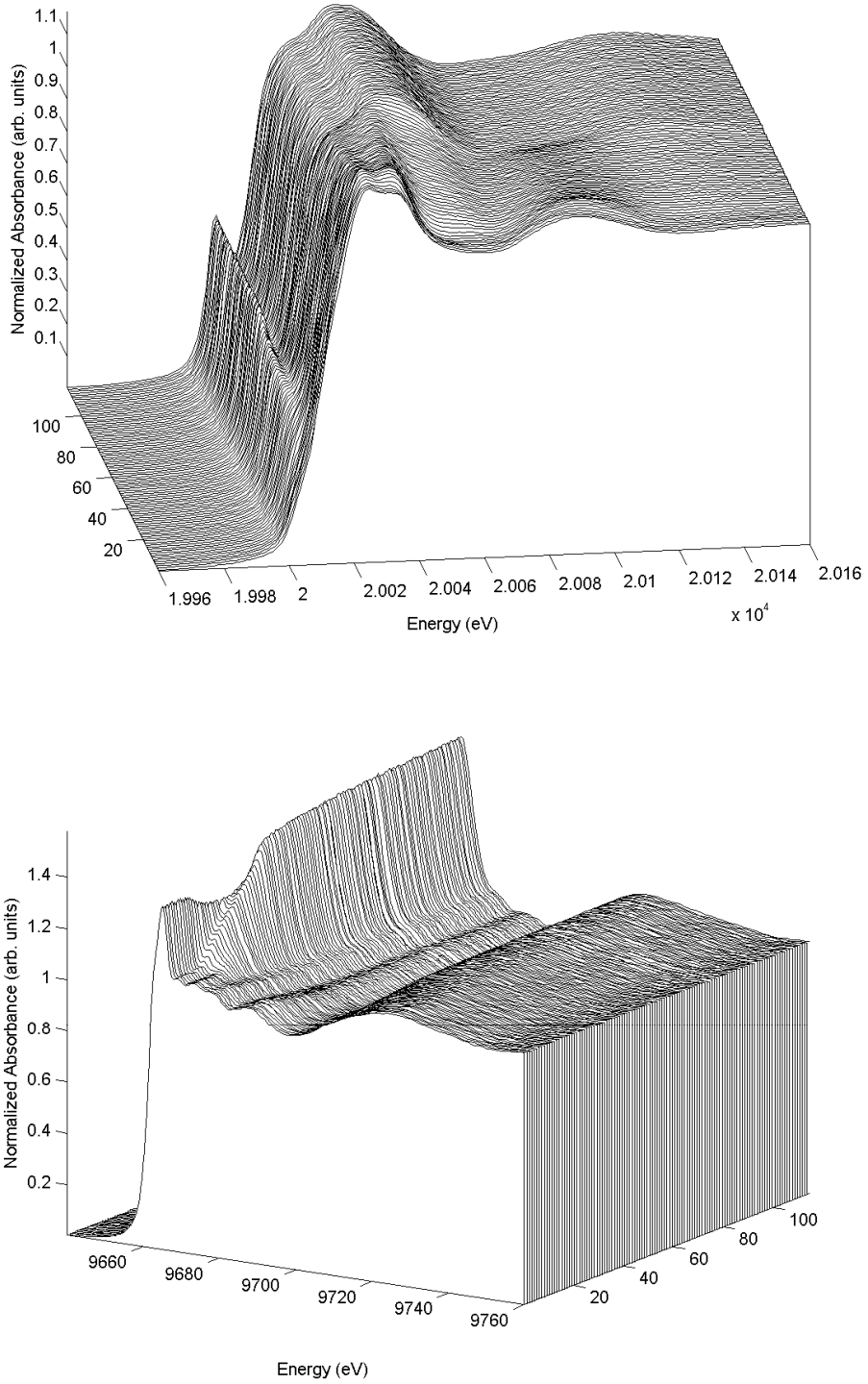

Fig. 8. Evolutions of time-resolved XANES spectra at Mo K-edge (up) and Zn K-edge (down) during the *in-situ* oxidative regeneration of the sulfided ZnO-MoO_3 materials physical mixture, under 5% O_2 in N_2 at 500°C.

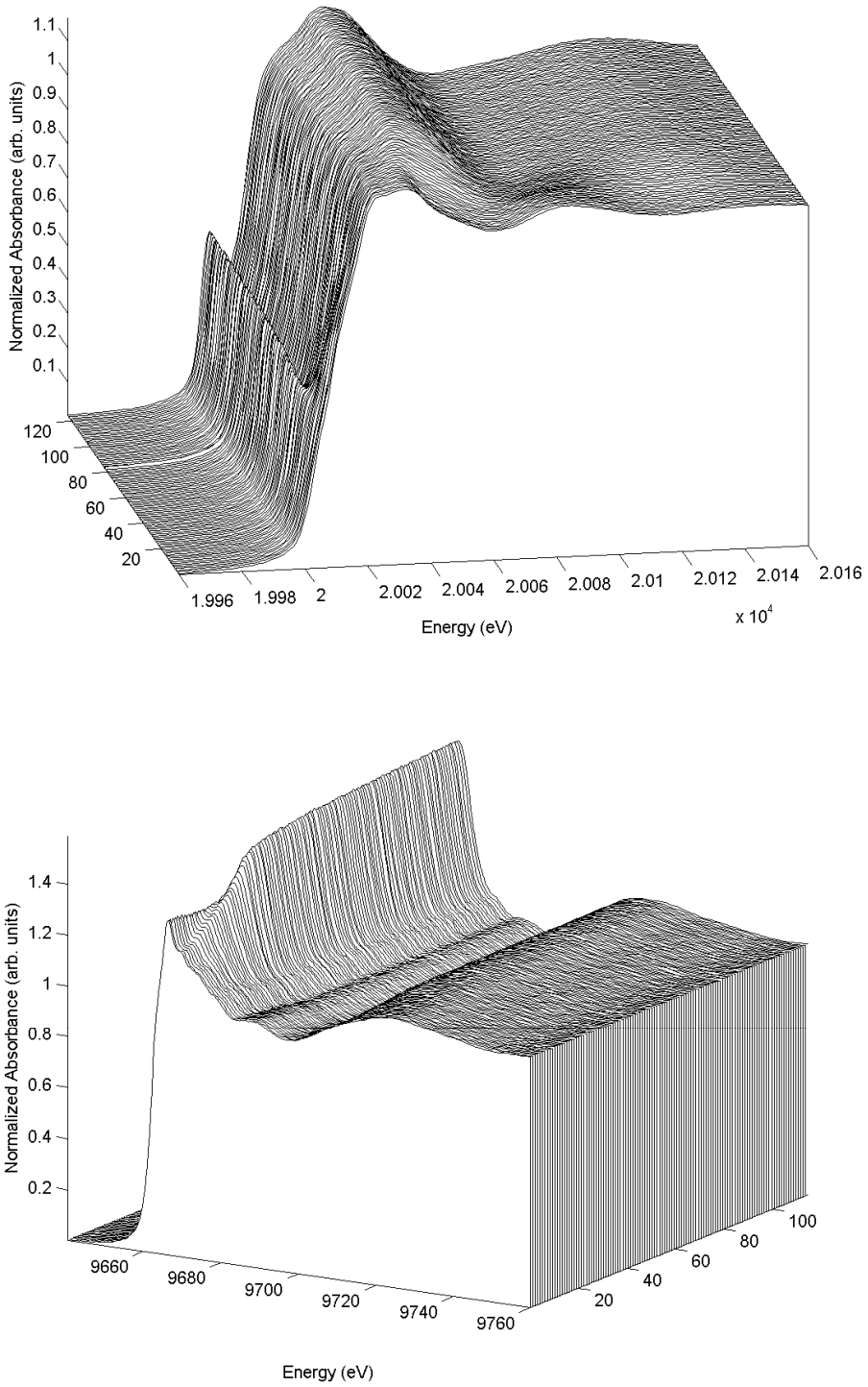

Fig. 9. Evolutions of time resolved XANES spectra at Mo K-edge (up) and Zn K-edge (down) during the *in-situ* oxidative regeneration of the sulfided $ZnMoO_4$ material, under 5% O_2 in N_2 at 500°C.

The concentration profiles obtained from MCR-ALS methodology applied to the XAS spectra recorded at both Mo and Zn K-edges during the regeneration step of sulfided ZnO-MoO_3

materials are reported on Fig. 10 and Fig. 11 respectively. Upon regeneration a much complex reaction scheme is involved, combining several gas-solid and solid-solid reactions.

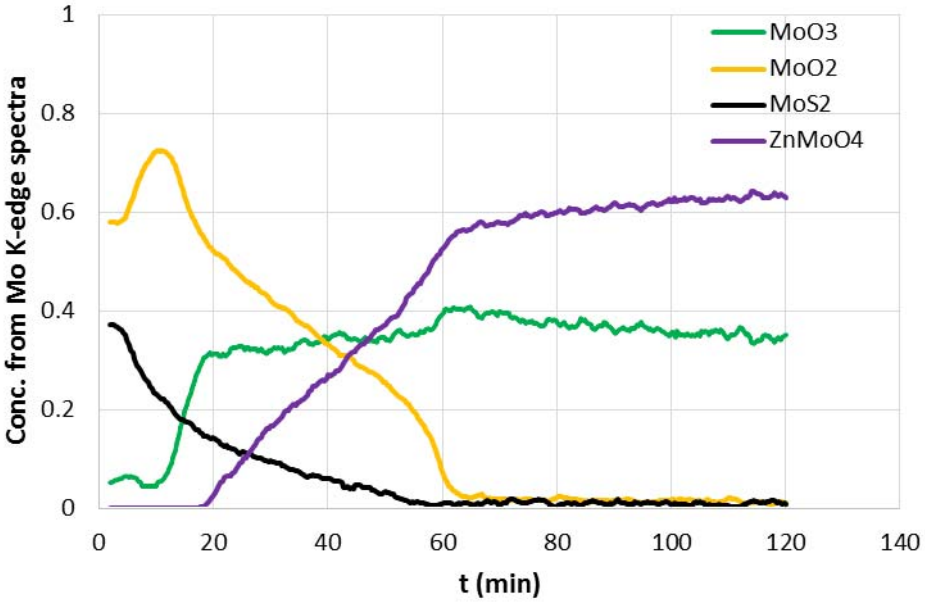

Fig. 10. MCR-ALS determination of concentration profiles as a function of time of Mo compounds (QXAS at Mo K-edge, 358 spectra) during the regeneration of sulfided MoO_3-ZnO mixture.

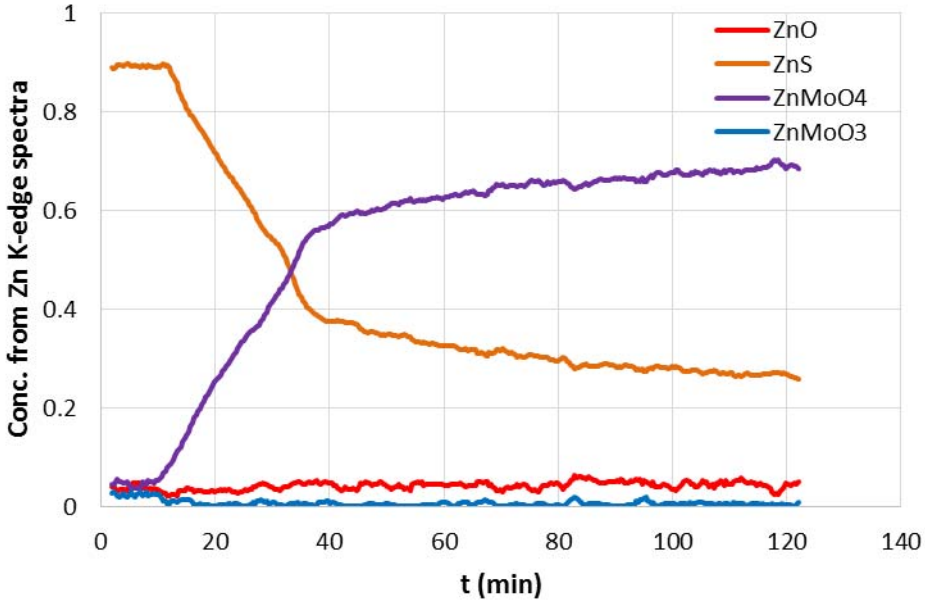

Fig. 11. MCR-ALS determination of concentration profiles as a function of time of Zn compounds (QXAS at Zn K-edge, 358 spectra) during the regeneration of sulfided MoO_3-ZnO mixture.

During the oxidative regeneration of the sulfided ZnO-MoO_3, MoS_2 is firstly oxidized into MoO_2 according to the following reaction [59,60]:

$$MoS_2(s) + 3\ O_2(g) \rightarrow MoO_2(s) + 2\ SO_2(g) \quad (7)$$

then MoO_2 is oxidized into MoO_3 according to [46,61]:

$$MoO_2(s) + ½\ O_2(g) \rightarrow MoO_3(s) \quad (8)$$

In agreement with previous observations obtained from *in-situ* XRD experiments [26], the formation of $ZnMoO_4$ phase is observed later on from MCR-ALS applied to Mo K-edge spectra.

Comparing results from Zn K-edge measurements, slight discrepancies are observed regarding $ZnMoO_4$ formation time and rate. This might originate from slightly different operating conditions between both experiments performed at Mo and Zn K-edges, respectively (*e.g.* variation of sample amount or GHSV). Nevertheless, consistent results are obtained from Zn K-edge spectra. Direct formation of $ZnMoO_4$ seems to occur as ZnS consumption is observed. Re-oxidation of Zn species is rather slow and incomplete, ZnO phase is not detected at the early stage of the reaction. As *Sotani et al* followed the formation of $ZnMoO_4$ from ZnO and MoO_3 single oxides at 400°C [49], one may propose at this stage the direct formation of $ZnMoO_4$ from ZnS and MoO_3:

$$2\ ZnS(s) + 2\ MoO_3(s) + 3\ O_2(g) \rightarrow 2\ ZnMoO_4(s) + 2\ SO_2(g) \quad (9)$$

However, the mechanism of such a transformation should be elucidated or refined, *e.g.* with investigations at lower temperature.

The concentration profile evolutions during the regeneration step of sulfided $ZnMoO_4$ materials are reported on Fig. 12 and Fig. 13 for measurements at Mo K-edge and Zn K-edge, respectively. Concentration profile obtained from measurements at both edges show consistent trends in term of composition, phase formation time and rate.

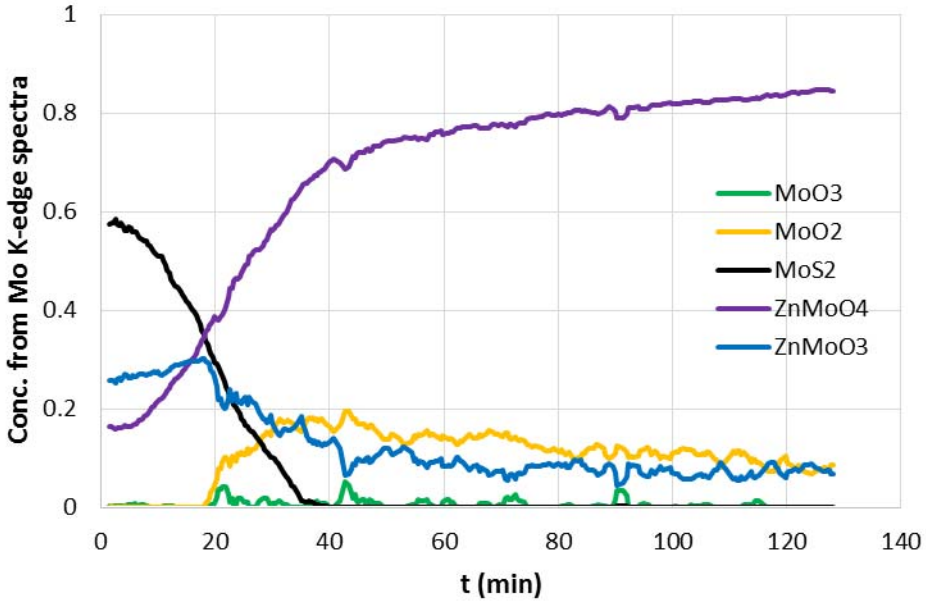

Fig. 12. MCR-ALS determination of concentration profiles as a function of time of Mo containing compounds (QXAS at Mo K-edge, 380 spectra) during the regeneration of sulfided $ZnMoO_4$ material.

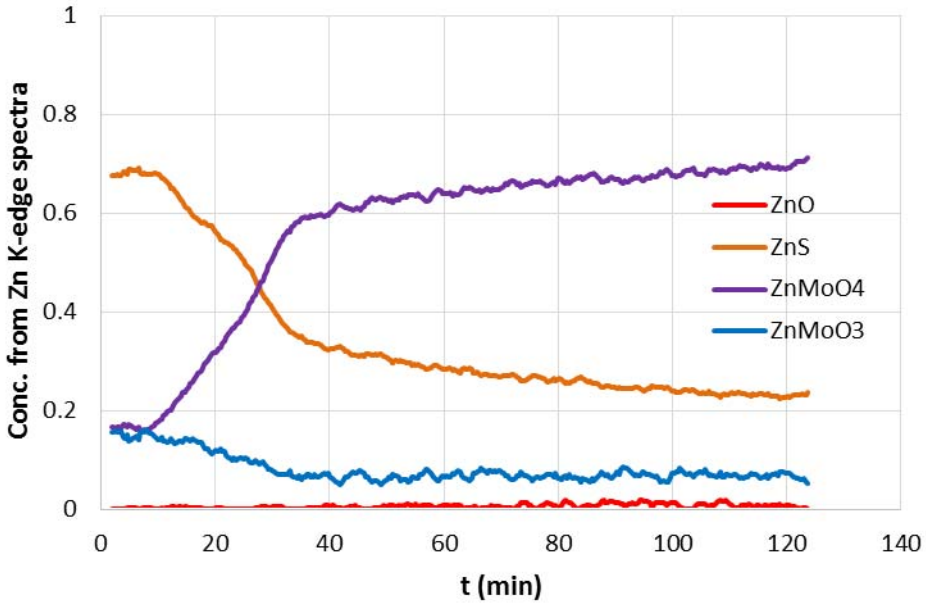

Fig. 13. MCR-ALS determination of concentration profiles as a function of time for Zn containing compounds (QXAS at Zn K-edge, 366 spectra) during the regeneration of sulfided $ZnMoO_4$ material.

Previous *in-situ* XRD study evidenced only traces of $ZnMoO_4$ and MoO_2 at the early stages of the regeneration [26]. Fig. 12 and Fig. 13 evidence a fast reaction of both MoS_2 and

ZnS sulfide phases, and concomitant formation of $ZnMoO_4$ and the absence of oxide intermediates. This rapid event can be summarized by the following equation:

$$MoS_2(s) + ZnS(s) + 5\ O_2(g) \rightarrow ZnMoO_4(s) + 3\ SO_2(g) \quad (4)$$

A fraction of initial $ZnMoO_3$ is also re-oxidized into $ZnMoO_4$.

However, as shown on Fig. 12, formation of MoO_2 is observed later on as a parallel route of re-oxidation of MoS_2. Reaction process and kinetics differ from regeneration of sulfided ZnO-MoO_3 mixture, where direct formation of $ZnMoO_4$ from MoO_3 and ZnS was observed. The absence of MoO_3 at the advanced stage of regeneration suggests that large particles of MoO_2 are present, these particles being reluctant to react with ZnS(/ZnO) to produce the ternary oxide. Therefore, the complete recovery of the initial $ZnMoO_4$ phase is not achieved. ZnS phase is remaining after regeneration according to MCR-ALS, although previously reported *in-situ* XRD and TGA regeneration experiments did not evidence detectable amounts of ZnS phase [26]. As for sulfidation reactions, materials oxidation involves solid-state diffusion phenomena leading to kinetics hindrance, potentially responsible for the incomplete transformation. Incomplete regeneration observed from QXAS experiments for this material might also result from operating conditions discrepancies such as those resulting from different cell configurations (different gas flow rate to solid amount ratio, preferred paths, …).

To conclude on the comparison of the activation/regeneration stages of the two systems, thanks to QXAS, the reactions dynamic was recorded and the initial formation and consumption rates for the different phases were estimated (Table 1). This confirms faster consumption of $ZnMoO_4$ phase compared to ZnO-MoO_3 material during the sulfidation step. Formation rate of MoS_2 reaction products is also higher from $ZnMoO_4$ sulfidation. MoO_2 is also preferentially formed from MoO_3 in ZnO-MoO_3 mixture, compared to MoS_2 formation from the same material. $ZnMoO_4$ initial formation rates during regeneration stage are rather similar for both materials.

Table 1. Initial reactivity (phase consumption and formation rates) of the solids measured for the sulfidation reaction of ZnO-MoO_3 and $ZnMoO_4$ materials at 350°C and the oxidative regeneration at 500°C (averaged values obtained from Mo and Zn K-edges measurements are provided).

Initial phase	Phases formed or consumed	Reactivity of solids and products (initial rate of disappearance or production) µmol.min^{-1}	
		Sulfidation step	Regeneration step
$ZnMoO_4$	$ZnMoO_4$	-1.47	1.69
	$ZnMoO_3$	0.67	-0.27
	MoS_2	0.71	-2.22
	ZnS	0.89	-0.98
$ZnO\text{-}MoO_3$	MoO_3	-0.89	–
	ZnO	-0.62	–
	MoO_2	0.71	–
	MoS_2	0.18	–
	ZnS	0.62	-1.78
	$ZnMoO_4$	–	1.78

For both solids, the heat generated by the exothermic oxidation reactions of molybdenum compounds (MoS_2, MoO_3 and $ZnMoO_3$) might accelerate the kinetics of the ZnS oxidation and the formation of the mixed oxide phase $ZnMoO_4$ [26]. This effect is even more important as $ZnMoO_4$ formation is also exothermic (more than MoO_3 formation).

At the end of the oxidative regeneration step, the phases compositions reported in Table 2 also indicate that both solids contains ZnS, so the regeneration is not fully completed. For both materials, regeneration stage leads to the formation of $ZnMoO_4$. Higher final conversion to the ternary phase is obtained at when starting from initial $ZnMoO_4$. Regarding the $ZnO\text{-}MoO_3$ material, the incomplete regeneration observed is consistent with similar regeneration experiments conducted on the same material through thermogravimetry under reactive atmosphere and *in-situ* XRD, as from elemental analysis, which shown incomplete regeneration process [26]. Zn/Mo molar ratio calculated from QXAS data at both edges are also reported in Table 2. One can notice the good agreement between calculated Zn/Mo ratio and expected ratio (= 1).

Other species might have contributed to XAS spectra, even though not considered in the present study, such as for example zinc sulfate (surface oxidation), or zinc oxysulfide phases [62,63]. Infrared spectra of oxidized ZnS at 500°C (not reported) show the presence of surface $ZnSO_4$. However, attempts to introduce a contribution to experimental XAS spectra

due to $ZnSO_4$ failed, then it was not possible to evidence the formation of bulk $ZnSO_4$. Sulfate phases are also known for their thermal stability [64,65], and are very likely to hinder sulfur sorbent reoxidation process.

Table 2 Phases composition of the regenerated solid at the end of the oxidative regeneration step (compositions have been calculated considering data obtained at the two edges).

Initial material	Phases formed	Composition (% molar basis)
Regenerated ZnO-MoO_3	$ZnMoO_4$	50.1
	MoO_3	27.0
	ZnO	3.6
	$ZnMoO_3$	0
	ZnS	19.3
	Zn/Mo ratio	0.95
Regenerated $ZnMoO_4$	$ZnMoO_4$	65.8
	$ZnMoO_3$	6.3
	MoO_2	6.3
	ZnS	21.6
	Zn/Mo ratio	1.20

4. Conclusions

QXAS experiments bring a better understanding of the reactivity of two candidate materials as H_2S capture compounds, a physical mixture of two oxides (ZnO-MoO_3) and a mixed oxide ($ZnMoO_4$). Chemometric tools are helpful for the understanding of complex sulfidation/regeneration reactions involved.

Under sulfiding conditions, the ZnO-MoO_3 physical mixture reactivity is very similar to the combination of separate ZnO and MoO_3 phase reactivity. ZnO is sulfided into ZnS, whereas MoO_3 is mainly reduced into MoO_2 and slightly sulfided into MoS_2. Under the same conditions, sulfidation of $ZnMoO_4$ mixed oxide leads to a partial phase demixing into ZnS

and MoS_2, surrounding a $ZnMoO_3$ core. Moreover, the amount of MoS_2 is more than twice higher in the ternary solid than in the mixed composition.

During the oxidative regeneration of both sulfided solids at 500°C, the molybdenum phases are oxidized, and the heat released might initiate the ZnS oxidation reaction by accelerating its kinetics. Finally, the more complete regeneration of the sulfided $ZnMoO_4$ might be explained by a better homogeneity of the sulfide phases located at the surface of oxide particles and leading to a better use of the heat released.

Finally, $ZnMoO_4$ mixed oxide has been shown to exhibit attractive properties for synthesis gas regenerative desulfurization processes, as material regeneration is obtained at much lower temperature (ΔT ~250°C) compared to single oxide ZnO based sorbents [26]. This work included in a multi-technique approach also brings novel and rational insights on gas-solid reactions studied, helping for a better understanding of the solid-state transformation mechanisms involved in both sulfidation and oxidative regeneration processes. MCR-ALS interpretation of QXAS provides unique information on the dynamic of such complex gas-solid and solid-solid reactions. The strength of multivariate analyses is also illustrated in the present work, which allows for monitoring the dynamic evolution of materials composition on zinc and molybdenum basis, through the spectra recorded at both Zn and Mo K-edges.

Acknowledgments

The authors are grateful to SOLEIL committees for beam time allocated on the SAMBA beamline.

References

[1] D. Vallentin, Policy drivers and barriers for coal-to-liquids (CtL) technologies in the United States, Energy Policy 36 (2008) 3198–3211.

[2] O. Shinada, A. Yamada, Y. Koyama, The development of advanced energy technologies in Japan: IGCC: A key technology for the 21st century, Energy Conversion and Management 43 (2002) 1221–1233.

[3] M.J. Prins, K.J. Ptasinski, Janssen, Frans J. J. G., Exergetic optimisation of a production process of Fischer–Tropsch fuels from biomass, Fuel Processing Technology 86 (2005) 375–389.

[4] C. Higman, van der Burgt, Maarten, Gasification, 2nd ed., Gulf Professional Pub./Elsevier Science, Amsterdam, Boston, 2008.

[5] H. Schulz, Short history and present trends of Fischer–Tropsch synthesis, Applied Catalysis A: General 186 (1999) 3–12.

[6] van der Laan, Gerard P., Beenackers, A. A. C. M., Kinetics and selectivity of the Fischer–Tropsch synthesis: a literature review, Catalysis Reviews 41 (1999) 255–318.

[7] A. Steynberg, M. Dry (Eds.), Fischer-Tropsch Technology, 2004.

[8] D. Chiche, C. Diverchy, A.-C. Lucquin, F. Porcheron, F. Defoort, Synthesis gas purification, Oil & Gas Science and Technology 68 (2013) 707–723.

[9] E. Jallouli, J.-P. Larpin, M. Lambertin, J.-C. Colson, Corrosion of ferritic steels (Fe-Cr-Al) in sulfur vapor and H_2S/H_2 mixtures, Oxidation of Metals 11 (1977) 335–354.

[10] C.H. Bartholomew, Mechanisms of catalyst deactivation, Applied Catalysis A: General 212 (2001) 17–60.

[11] Ø. Borg, N. Hammer, B.C. Enger, R. Myrstad, O.A. Lindvåg, S. Eri, T.H. Skagseth, E. Rytter, Effect of biomass-derived synthesis gas impurity elements on cobalt Fischer–Tropsch catalyst performance including in situ sulphur and nitrogen addition, Journal of Catalysis 279 (2011) 163–173.

[12] S.S. Pansare, J.D. Allison, An investigation of the effect of ultra-low concentrations of sulfur on a Co/γ-Al_2O_3 Fischer–Tropsch synthesis catalyst, Applied Catalysis A: General 387 (2010) 224–230.

[13] J.F. Akyurtlu, A. Akyurtlu, Hot gas desulfurization with vanadium-promoted zinc ferrite sorbents, Gas Separation & Purification 9 (1995) 17–25.

[14] D. Karayilan, T. Dogu, S. Yasyerli, G. Dogu, Mn−Cu and Mn−Cu−V Mixed-Oxide Regenerable Sorbents for Hot Gas Desulfurization, Industrial & Engineering Chemistry Research 44 (2005) 5221–5226.

[15] R.J. Madon, H. Seaw, Effect of sulfur on the Fischer-Tropsch synthesis, Catalysis Reviews: Science and Engineering 15 (1977) 69–106.

[16] C.H. Bartholomew, R.M. Bowman, Sulfur poisoning of cobalt and iron Fischer-Tropsch catalysts, Applied Catalysis 15 (1985) 59–67.

[17] A.L. Kohl, R. Nielsen, Gas purification, 5th ed., Gulf Publishing, Houston, Texas, 1997.

[18] K. Weissermel, H.-J. Arpe, Industrial Organic Chemistry, 4th ed., Wiley-VCH, Weinheim, 2003.

[19] K. Polychronopoulou, A.M. Efstathiou, Effects of Sol−Gel Synthesis on 5Fe−15Mn−40Zn−40Ti−O Mixed Oxide Structure and its H_2S Removal Efficiency from Industrial Gas Streams, Environmental Science & Technology 43 (2009) 4367–4372.

[20] A. Giuffrida, M.C. Romano, G.G. Lozza, Thermodynamic assessment of IGCC power plants with hot fuel gas desulfurization, Applied Energy 87 (2010) 3374–3383.

[21] S. Cheah, D.L. Carpenter, K.A. Magrini-Bair, Review of Mid- to High-Temperature Sulfur Sorbents for Desulfurization of Biomass- and Coal-derived Syngas, Energy & Fuels 23 (2009) 5291–5307.

[22] Jorgensen, F. R. A., F.J. Moyle, Phases formed during the thermal analysis of pyrite in air, Journal of Thermal Analysis 25 (1982) 473–485.

[23] J.G. Dunn, C. Muzenda, Quantitative analysis of phases formed during the oxidation of covellite (CuS), Journal of Thermal Analysis and Calorimetry 64 (2001) 1241–1246.

[24] R. Dimitrov, I. Bonev, Mechanism of zinc sulphide oxidation, Thermochimica Acta 106 (1986) 9–25.

[25] V. Girard, A. Baudot, D. Chiche, D. Bazer-Bachi, C. Bounie, C. Geantet, Rational selection of single oxide sorbents for syngas desulfurization regenerable at reduced temperature: Thermochemical calculations and experimental study, Fuel 128 (2014) 220–230.

[26] V. Girard, D. Chiche, A. Baudot, D. Bazer-Bachi, I. Clémençon, F. Moreau, C. Geantet, Innovative low temperature regenerable zinc based mixed oxide sorbents for synthesis gas desulfurization, Fuel 140 (2015) 453–461.

[27] R. Dimitrov, B. Boyanov, Investigation of the oxidation of metal sulphides and sulphide concentrates, Thermochimica Acta 64 (1983) 27–37.

[28] P.R. Westmoreland, D.P. Harrison, Evaluation of candidate solids for high-temperature desulfurization of low-Btu gases, Environmental Science & Technology 10 (1976) 659–661.

[29] W.F. Elseviers, H. Verelst, Transition metal oxides for hot gas desulphurisation, Fuel 78 (1999) 601–612.

[30] R. Frahm, Quick scanning EXAFS: First experiments, Nuclear Instruments and Methods in Physics Research Section A: Accelerators, Spectrometers, Detectors and Associated Equipment 270 (1988) 578–581.

[31] J. Stötzel, D. Lützenkirchen-Hecht, R. Frahm, A new flexible monochromator setup for quick scanning x-ray absorption spectroscopy, The Review of Scientific Instruments 81 (2010) 73109.

[32] E. Fonda, A. Rochet, M. Ribbens, L. Barthe, S. Belin, V. Briois, The SAMBA quick-EXAFS monochromator: XAS with edge jumping, Journal of Synchrotron Radiation 19 (2012) 417–424.

[33] C. La Fontaine, L. Barthe, A. Rochet, V. Briois, X-ray absorption spectroscopy and heterogeneous catalysis: Performances at the SOLEIL's SAMBA beamline, Catalysis Today 205 (2013) 148–158.

[34] Lesage C., E. Devers, C. Legens, G. Fernandes, O. Roudenko, V. Briois, High Pressure Cell for Edge Jumping X-ray Absorption Spectroscopy: Applications to industrial liquid sulfidation of hydrotreatment catalysts, Catalysis Today, Special Issue of Operando VI Submitted.

[35] R. Tauler, Multivariate curve resolution applied to second order data, Chemometrics and Intelligent Laboratory Systems 30 (1995) 133–146.

[36] W.H. Cassinelli, L. Martins, A.R. Passos, S.H. Pulcinelli, C.V. Santilli, A. Rochet, V. Briois, Multivariate curve resolution analysis applied to time-resolved synchrotron X-ray Absorption Spectroscopy monitoring of the activation of copper alumina catalyst, Catalysis Today 229 (2014) 114–122.

[37] A. Voronov, A. Urakawa, W. van Beek, N.E. Tsakoumis, H. Emerich, M. Rønning, Multivariate curve resolution applied to in situ X-ray absorption spectroscopy data: An efficient tool for data processing and analysis, Analytica Chimica Acta 840 (2014) 20–27.

[38] A. Martini, E. Borfecchia, K.A. Lomachenko, I.A. Pankin, C. Negri, G. Berlier, P. Beato, H. Falsig, S. Bordiga, C. Lamberti, Composition-driven Cu-speciation and reducibility in Cu-CHA zeolite catalysts: a multivariate XAS/FTIR approach to complexity, Chemical Science 8 (2017) 6836–6851.

[39] A. Rochet, B. Baubet, V. Moizan, E. Devers, A. Hugon, C. Pichon, E. Payen, V. Briois, Intermediate Species Revealed during Sulfidation of Bimetallic Hydrotreating Catalyst: A Multivariate Analysis of Combined Time-Resolved Spectroscopies, The Journal of Physical Chemistry C 121 (2017) 18544–18556.

[40] J. Jaumot, R. Gargallo, A. de Juan, R. Tauler, A graphical user-friendly interface for MCR-ALS: a new tool for multivariate curve resolution in MATLAB, Chemometrics and Intelligent Laboratory Systems 76 (2005) 101–110.

[41] J. Jaumot, A. de Juan, R. Tauler, MCR-ALS GUI 2.0: New features and applications, Chemometrics and Intelligent Laboratory Systems 140 (2015) 1–12.

[42] A. Rochet, B. Baubet, V. Moizan, C. Pichon, V. Briois, Co-K and Mo-K edges Quick-XAS study of the sulphidation properties of Mo/Al_2O_3 and $CoMo/Al_2O_3$ catalysts, Comptes Rendus Chimie 19 (2016) 1337–1351.

[43] T. Ressler, Jentoft, R. E., J. Wienold, Günter, M. M., O. Timpe, In Situ XAS and XRD Studies on the Formation of Mo Suboxides during Reduction of MoO_3, The Journal of Physical Chemistry B 104 (2000) 6360–6370.

[44] T. Ressler, O. Timpe, T. Neisius, J. Find, G. Mestl, M. Dieterle, R. Schlögl, Time-Resolved XAS Investigation of the Reduction/Oxidation of MoO_{3-x}, Journal of Catalysis 191 (2000) 75–85.

[45] L. Medici, R. Prins, The Influence of Chelating Ligands on the Sulfidation of Ni and Mo in $NiMo/SiO_2$ Hydrotreating Catalysts, Journal of Catalysis 163 (1996) 38–49.

[46] L. Li, M.R. Morrill, H. Shou, D.G. Barton, D. Ferrari, R.J. Davis, P.K. Agrawal, C.W. Jones, D.S. Sholl, On the Relationship between Mo K-Edge Energies and DFT Computed Partial Charges, The Journal of Physical Chemistry C 117 (2013) 2769–2773.

[47] T.S. Nguyen, S. Loridant, L. Chantal, T. Cholley, C. Geantet, Effect of glycol on the formation of active species and sulfidation mechanism of $CoMoP/Al_2O_3$ hydrotreating catalysts, Applied Catalysis B: Environmental 107 (2011) 59–67.

[48] S.C. Abrahams, Crystal Structure of the Transition-Metal Molybdates and Tungstates. III. Diamagnetic α-$ZnMoO_4$, The Journal of Chemical Physics 46 (1967) 2052–2063.

[49] N. Sotani, T. Suzuki, K. Nakamura, K. Eda, S. Hasegawa, Change in bulk and surface structure of mixed MoO_3-ZnO oxide by heat treatment in air and in hydrogen, Journal of Materials Science 36 (2001) 703–713.

[50] C. Guglieri, J. Chaboy, Characterization of the ZnO−ZnS Interface in THIOL-Capped ZnO Nanoparticles Exhibiting Anomalous Magnetic Properties, The Journal of Physical Chemistry C 114 (2010) 19629–19634.

[51] B. Gilbert, B.H. Frazer, H. Zhang, F. Huang, J.F. Banfield, D. Haskel, J.C. Lang, G. Srajer, G.D. Stasio, X-ray absorption spectroscopy of the cubic and hexagonal polytypes of zinc sulfide, Physical Review B 66 (2002) 245205.

[52] K. Ławniczak-Jabłońska, R.J. Iwanowski, Z. Gołacki, A. Traverse, S. Pizzini, A. Fontaine, Correlation between XANES of the transition metals in ZnS and ZnSe and their limit of solubility, Physica B: Condensed Matter 208–209 (1995) 497–499.

[53] A. Manthiram, J. Gopalakrishnan, New $A^{2+}Mo^{4+}O_3$ oxides with defect spinel structure, Materials Research Bulletin 15 (1980) 207–211.

[54] J.C. Gautherin, F. Le Boete, J.C. Colson, Etude cinétique et morphologique de la sulfuration de quelques oxydes de tungstène et de molybdène par le sulfure d'hydrogène, Journal de Chimie Physique 71 (1974) 771–776.

[55] J.M. Zabala, P. Grange, B. Delmon, Sur la réduction-sulfuration de l'anhydrique molybdique en présence de sulfure d'hydrogène, Comptes Rendus de l'Académie des Sciences - Series C 279 (1974) 725–728.

[56] L. Neveux, D. Chiche, D. Bazer-Bachi, L. Favergeon, M. Pijolat, New insight on the ZnO sulfidation reaction: Evidences for an outward growth process of the ZnS phase, Chemical Engineering Journal 181-182 (2012) 508–515.

[57] L. Neveux, D. Chiche, J. Pérez-Pellitero, L. Favergeon, A.S. Gay, M. Pijolat, New insight into the ZnO sulfidation reaction: mechanism and kinetics modeling of the ZnS outward growth, Physical Chemistry Chemical Physics 15 (2013) 1532–1545.

[58] A. Steinbrunn, C. Lattaud, RHEED and Auger study of the MoO_3(010) surface interaction with H_2S/H_2 mixture and pure H_2S, Surface Science 155 (1985) 279–295.

[59] Ž.D. Živković, J. Šesták, Kinetics and Mechanism of the Oxidation of Molybdenum Sulphide, Journal of Thermal Analysis and Calorimetry 53 (1998) 263–267.

[60] Y. Yoshimura, T. Sato, H. Shimada, N. Matsubayashi, M. Imamura, A. Nishijima, S. Yoshitomi, T. Kameoka, H. Yanase, Oxidative Regeneration of Spent Molybdate and Tungstate Hydrotreating Catalysts, Energy & Fuels 8 (1994) 435–445.

[61] T. Ressler, J. Wienold, Jentoft, R. E., O. Timpe, T. Neisius, Solid state kinetics of the oxidation of MoO_2 investigated by time-resolved X-ray absorption spectroscopy, Solid State Communications 119 (2001) 169–174.

[62] A.N. Salak, O.V. Ignatenko, A.L. Zhaludkevich, A.D. Lisenkov, M. Starykevich, M.L. Zheludkevich, M.G.S. Ferreira, High-pressure zinc oxysulphide phases in the ZnO–ZnS system, Physica Status Solidi A 212 (2015) 791–795.

[63] A.L. Dadlani, S. Acharya, O. Trejo, F.B. Prinz, J. Torgersen, ALD Zn(O,S) thin films' interfacial chemical and structural configuration probed by XAS, ACS Applied Materials & Interfaces 8 (2016) 14323–14327.

[64] J.G. Dunn, The oxidation of sulphide minerals, Thermochimica Acta 300 (1997) 127–139.

[65] R.V. Siriwardane, J.A. Poston, G. Evans, Spectroscopic Characterization of Molybdenum-Containing Zinc Titanate Desulfurization Sorbents, Industrial & Engineering Chemistry Research 33 (1994) 2810–2818.